Phys Chem Minerals (2004) 31: 475–486
DOI 10.1007/s00269-004-0398-7

ORIGINAL PAPER

V. Botella† · V. Timon · E. Escamilla-Roa
A. Hernández-Laguna · C. I. Sainz-Díaz

Hydrogen bonding and vibrational properties of hydroxy groups in the crystal lattice of dioctahedral clay minerals by means of first principles calculations

Received: 14 July 2003 / Accepted: 8 April 2004

Abstract The hydroxy groups of the crystal lattice of dioctahedral 2:1 phyllosilicates were investigated by means of quantum-mechanical calculation. The standard Kohn-Sham self-consistent density functional theory (DFT) method was applied using the generalized gradient approximation (GGA) with numerical atomic orbitals and double-zeta polarized functions as basis set. Isomorphous cation substitution of different cations in the octahedral and tetrahedral sheet was included along with several interlayer cations reproducing experimental crystal lattice parameters. The effect of these substitutions and the interlayer charge on the hydroxyl group properties was also studied. These structures represent different cation pairs among Al^{3+}, Fe^{3+} and Mg^{2+} in the octahedral sheet of clays joined to OH groups. The geometrical disposition of the OH bond in the crystal lattice and the hydrogen bonds and other electrostatic interactions of this group were analyzed. The frequencies of different vibrational modes of the OH group [ν(OH), δ(OH) and γ(OH)] were calculated and compared with experimental data, finding a good agreement. These frequencies depend significantly on the nature of cations which are joined with, and the electrostatic interactions with, the interlayer cations. Besides, hydrogen-bonding interactions with tetrahedral oxygens are important for the vibrational properties of the OH groups; however, also the electrostatic interactions of these OH groups with the rest of tetrahedral oxygens within the tetrahedral cavity should be taken into account. The cation substitution effect on the vibration modes of the OH groups was analyzed reproducing the experimental behaviour.

Keywords Smectites · Quantum mechanics · Vibration frequencies · Hydrogen bonds

V. Botella · V. Timon
Instituto de Estructura de la Materia (CSIC),
C/Serrano, 113(bis), 28006 Madrid, Spain

Present address: V. Timon
Science Labs.,
University of Durham, South Road,
Durham DH1 3LE, UK

E. Escamilla-Roa · A. Hernández-Languna · C.I. Sainz-Díaz (✉)
Estación Experimental del Zaidín (CSIC),
C/ Profesor Albareda 1, 18008-Granada, Spain
E-mail: sainz@eez.csic.es

†Dr. V. Botella passed away last February

Introduction

Clay minerals are important in cosmetics, oil drilling, toxic and radioactive waste disposal, catalysis, drug and agrochemical delivery, as additives for polymeric materials etc. These minerals play a key role in the fate and mobility of contaminants in natural systems, and they are especially interesting as barrier in nuclear waste deposits.

The 2:1 phyllosilicates have a layer structure where two tetrahedral layers sandwich a sheet of octahedrally coordinated cations. These minerals present a great diversity of compounds because of their capacity for isomorphous substitution, Al^{3+} by Mg^{2+}, Fe^{3+}, and Fe^{2+} in the octahedral sheet, and Si^{4+} by Al^{3+} in the tetrahedral sheet. These substitutions can produce a negative charge that is compensated by the presence of cations in the interlayer space (Brindley and Brown 1984). Many XRD studies of 2:1 clay structures are reported, but they give no indication of the proton positions within the hydroxyl groups. Although using techniques of neutron diffraction they have been able to obtain some meaningful results in mica minerals (Catti et al. 1994). The study of the structure and properties of these hydroxyl groups is interesting, because they can play a major role in the catalytic activity of these minerals, and in their interactions with water, other molecules and cations. Additionally, the octahedral cations can play a significant role in sorption and dissolution phenomena in many minerals, where OH groups can have varying effects on the reactivity of mineral surface (Schindler and Stumm 1987).

Spectroscopic IR analyses of clay minerals are very useful and they can yield information about the stretching, ν(OH), and bending, δ(OH), vibrations of the OH groups. These vibrations are highly dependent on the cations joined to these OH groups and some relationships between IR spectra and crystal structure can be found (Cuadros et al. 1999). However, the mechanism that governs the OH fundamental vibrations observed experimentally is not fully understood yet and some discrepancies are found (Vedder 1964; Robert and Kodama 1988; Madejová et al. 1994; Besson and Drits 1997). Recently, Pelletier et al. (2003) applied IR and Raman analyses to trioctahedral clay minerals (saponites), observing an increase in the ν(OH) frequency with the layer charge and a variation in the ν(OH) frequency of the structural hydroxyl group with the hydration degree. Therefore, the high diversity in cation composition and cation distribution, the high disorder degree between layers and the approaches used for interpretation of the experimental results make the experimental analysis of these vibrations very difficult. A theoretical approach by means of computational calculations can be very useful to interpret the experimental behaviour. Quantum-mechanical works on molecular clusters of these mineral structures have been reported including OH vibration studies (Kubicki and Apitz 1998, Sainz-Díaz et al. 2000, Timón et al. 2003), however, this approach is limited by the edge effects of the cluster model. First-principles calculations of the whole periodical crystal lattice of phyllosilicates have also been reported (Sainz-Díaz et al. 2002; Hobbs et al. 1997; Boek and Sprik 2003). The aim of this work is to find a theoretical approach at DFT quantum-mechanical level to investigate the hydrogen bond interactions of the OH groups, and the OH vibrations in the dioctahedral 2:1 phyllosilicate crystal lattice in a wide range of cation substitutions.

Methodology

Numerical atomic orbital methodology was used for the total energy calculations based on density functional theory (DFT) and pseudopotentials implemented in the SIESTA program (Sánchez-Portal et al. 1997; Artacho et al. 1999). It is a method that scales linearly with the number of atoms in the simulation cell. The Perdew–Burke–Ernzerhof parameterization of the exchange-correlation functional was used (Perdew et al. 1996). The generalized gradient approximation (GGA) was used, since it has been reported that hydrogen-bonded systems are better described using gradient-corrected exchange-correlation functionals (Lee et al. 1993). The basis sets are made of strictly localized numerical atomic orbitals (NAOs). Their localization cutoff radii correspond to an energy shift of 270 meV. The basis sizes used in this work are double-zeta polarized (DZP) following the perturbative polarization scheme (Artacho et al. 1999).

A uniform mesh with certain plane-wave cutoff energy was used to represent the electron density, the local part of the pseudopotential and the Hartree and exchange-correlation potentials. Core electrons have been replaced by norm-conserving pseudopotentials (Troullier and Martins 1991) factorized in the Kleinman–Bylander form (Kleinman and Bylander 1982), including scalar-relativistic effects (Bachelet and Schluter 1982) and non-linear partial-core corrections (Louie et al. 1982) in some cases. The pseudopotentials simulate the interaction between the valence electrons and the cores (nuclei plus core electrons) and neither core electrons nor core wave-functions have to be included explicitly. With this approximation the valence wave functions are substituted by pseudo-wave functions that do not present strong oscillations in the core region. In the case of potassium, a partial core correction (Louie et al. 1982) was used, since it was shown to be necessary for alkali metal elements (Hebenstreit and Scheffler 1992). The same correction was applied for the iron atoms. In atoms, iron and potassium, scalar relativistic effects were included. Calculations were restricted to the Γ point in the Brillouin zone, since previous work (Stich et al. 1996) found cell-size effects to be small. In all structures, all atoms and all cell parameters have been relaxed using the forces and the stress tensor by means of conjugated gradient minimizations. More details about the calculation conditions are reported elsewhere (Sainz-Díaz et al. 2002). Vibrational modes and frequencies were obtained from the force constant analysis calculated with the SIESTA program. The analysis of frequencies of the vibrational modes has been performed by means of the program package VIBRA (Soler et al. 2002). This work presents the main three vibrational modes of the OH groups: stretching ν(OH) bending in-plane δ(OH), and bending out-of-plane γ(OH).

In the study of the crystal lattice of dioctahedral 2:1 phyllosilicates, a periodic model is designed with an octahedral layer joined to two tetrahedral layers and an interlayer space. Then our crystal model is composed by a unit cell of these minerals. This structure will represent all the mineral repeating n times by translational symmetry operations along the crystallography axis a, b and c. This model (Fig. 1) contains the most relevant and closer features to study the effect of the isomorphous cation substitution in the octahedral sheet on the OH vibration frequencies.

Different compositions are studied in this work (Table 1). This series tries to cover a wide range of tetrahedral, octahedral and interlayer (IC) charges, including pyrophyllite (no significant IC), smectites (low IC, mainly from octahedral sheet) and illites (medium IC, mainly from tetrahedral sheet). Different interlayer cations are included (Na^+ and K^+). Different cation substitutions of Si^{4+} by Al^{3+} in the tetrahedral sheet and Al^{3+} by Mg^{2+} and Fe^{3+} in the octahedra are considered. In this series, there are samples without tetrahedral charge, samples with a certain tetrahedral charge, samples without octahedral charge (end member of beidellite) and samples with high octahedral charge. Samples with a high Fe^{3+} content in the octahedral sheet are also included. All samples are in a dry state with no water molecule in the interlayer space.

The pyrophyllite experimental structural data were taken from X-ray diffraction studies (Lee and Guggenheim 1981). In the smectite/illite samples, no experimental atomic coordinate set was available. Nevertheless, the initial geometries were taken from the models proposed by Tsipursky and Drits (1984) based on oblique-texture electron diffraction studies of dioctahedral smectites. The optimized structures have been reported elsewhere (Sainz-Díaz et al. 2002).

Results and discussion

Full geometry optimizations were done using unit cells (40–43 atoms). These calculations reproduce the experimental values of the main crystal lattice parameters of these clay minerals (Table 2, for more details see Sainz-Díaz et al. 2002). The exchange of Na^+ by K^+ as interlayer cation does not produce significant differences in the lattice geometry of these minerals. The calculated values of the a parameter match the experiment in pyrophyllite, although they are slightly lower than experimental values in illite/smectite sample. The presence of Fe^{3+} in the octahedral sheet produces a slight

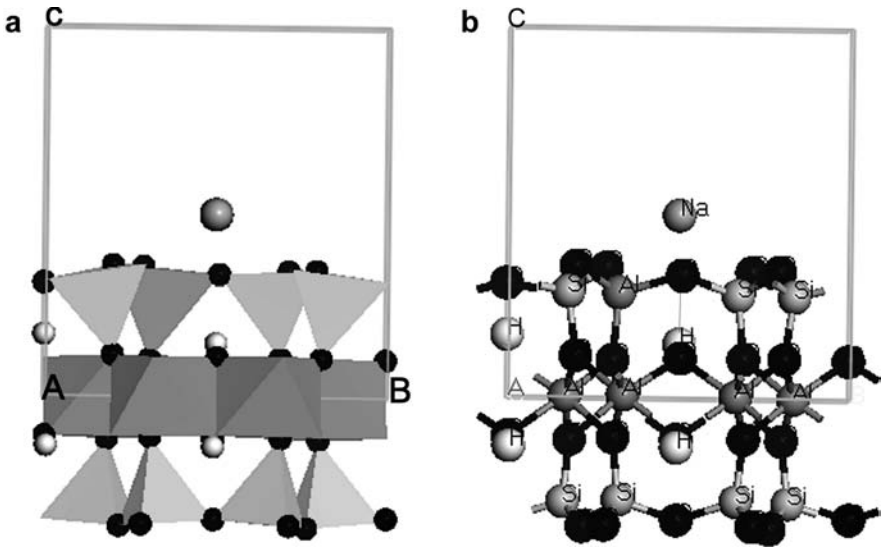

Fig. 1 Crystal structure of dioctahedral 2:1 phyllosilicates

Table 1 Chemical composition of the clay samples studied. Structural formulae on the basis O_{20} $(OH)_4$ (T tetrahedral; Oc octahedral)

Structure	Si^{4+} (T)	Al^{3+} (T)	Al^{3+} (Oc)	Mg^{2+} (Oc)	Fe^{3+} (Oc)	Interlayer cation
Pyrophyllite	8		4			
$Smec_1$	7	1	4			Na^+
$Smec_2$	7	1	4			K^+
$Smec_3$	7	1	2		2	Na^+
$Smec_4$	7	1	2		2	K^+
$Smec_5$	8		2	2		$2K^+$
$Smec_6$	8		3	1		K^+
$Smec_7$	8		2	1	1	K^+
$Smec_8$	7	1	3		1	K^+

decrease in the *b*, *c* and *β* parameters but within the experimental range. The samples with Mg^{2+} in the octahedral sheet present higher M–O and M–OH bond lengths than in the rest of samples, due to the greater ionic radius of Mg^{2+} than that of Al^{3+}. However, samples with Fe^{3+}, that has a similar ionic radius to Mg^{2+}, do not present long M–O and M–OH bond lengths. Therefore, the negative charge generated by the Mg^{2+} substitution in the surrounding O atoms should also play an important role in this phenomenon.

Geometry and interactions of the OH groups

The position of hydrogen atoms in the crystal is difficult to localize experimentally. In this work we analyze the spatial disposition of the OH bonds in the cage of surrounding O atoms, and their interactions in the crystal lattice of dioctahedral 2:1 phyllosilicates. The position of the H atom of the OH group depends on the electrostatic interactions with the surrounding O atoms and the interlayer cation. This H atom can form hydrogen bonds

Table 2 Calculated and experimental lattice parameters of the clay samples studied (lengths and angles in degrees)

Sample	*a*	*b*	*c*	*β*	d(O–H)[a]	d(M–O)[a,b]
Exp [c]	5.18	8.97–9.01	10.05–10.2	99.6–101.4	0.95	1.94
Pyro[d]	5.15 (5.16)	8.98	9.21 (9.35)	99.8	0.977	1.94 (1.90)
$Smec_1$	5.12	9.06	10.10	101.2	0.979	1.96 (1.91)
$Smec_2$	5.12	9.06	10.08	101.6	0.979	1.95 (1.91)
$Smec_3$	5.14	9.01	10.01	101.9	0.991	1.95 (1.90)
$Smec_4$	5.12	8.98	9.95	101.9	0.992	1.95 (1.89)
$Smec_5$	5.16	9.08	10.05	100.9	0.981	2.02 (1.97)
$Smec_6$	5.13	9.05	10.06	101.2	0.978	2.00 (1.95)
$Smec_7$	5.11	8.98	9.89	101.4	0.986	1.96 (1.96)
$Smec_8$	5.10	9.00	9.98	101.8	0.984	1.95 (1.92)

[a]Mean values
[b]*d*(M–OH) values in brackets
[c]Experimental values of illite-smectites (Tsipursky and Drits 1984) and *d*(O–H) and *d*(M–O) bond lengths were taken from muscovite data (Guggenheim et al 1987).
[d]Pyrophyllite, experimental values are *in brackets* when they are different from the above row (Lee and Guggenheim 1981)

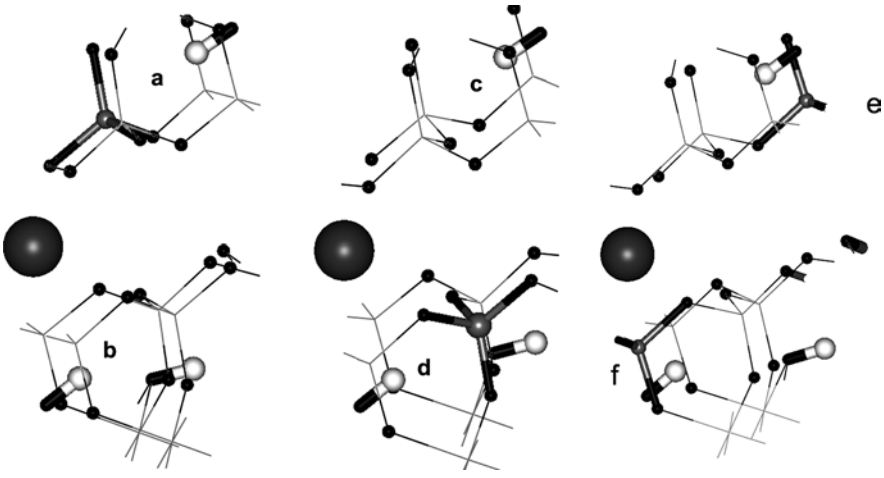

Fig. 2a–f Possible configurations of the OH groups in the crystal lattice of dioctahedral phyllosilicates. **a** $(OH)_{\varnothing,Al}$ with the Al in the tetrahedral that are in front of the OH. **b** $(OH)_{IC,\varnothing}$. **c** $(OH)_{\varnothing,\varnothing}$. **d** $(OH)_{IC,Al}$ with the Al in the tetrahedral that are in front of the OH. **e** $(OH)_{\varnothing,Al}$ with the Al in lateral tetrahedra. **f** $(OH)_{IC,Al}$ with the Al in lateral tetrahedra. *White*, *black* and *grey circles* represent H, O and tetrahedral Al atoms, respectively. The *large ball* represents the interlayer cation

and weaker attractive electrostatic interactions with the basal and apical tetrahedral O atoms, and can also have electrostatic repulsion with the interlayer cation throughout the hexagonal tetrahedral cavity. All these interactions will also depend on the isomorphous cation substitutions in the tetrahedral and octahedral sheets, the interlayer cation and the distribution of all these cations with respect to these OH groups. Hence, different orientations of the OH groups can be found in a phyllosilicate layer for a certain cation composition. This was observed experimentally in trioctahedral clays (saponites) by means of Raman spectroscopy (Pelletier et al. 2003).

In these crystalline systems, we have four OH groups per unit cell. In pyrophyllite all the OH groups are equivalent because there is no cation substitution and no interlayer cation. However, in most illite smectites these OH groups are not equivalent at all, because there are hexagonal tetrahedral cavities with or without IC, and the tetrahedral Al atom can be closed up or far away to the OH groups. This means that in some models the tetrahedral cation substitution is one Al cation per unit cell that will be in only one tetrahedral sheet. Therefore, some OH groups will be oriented towards the tetrahedral sheet with the Al substitution $[(OH)_{x,Al}]$ or towards another tetrahedral sheet $[(OH)_{x,\varnothing}]$. Besides, taking into account the position related to the IC, we have to define these OH groups as: those located in the cavity with interlayer cation (IC) $[(OH)_{IC,y}]$ and that can be close or not to the tetrahedral Al, ^{IV}Al, cation [$(OH)_{IC,Al}$ and $(OH)_{IC,\varnothing}$, respectively], and those that are not located in the cavity with interlayer cation $[(OH)_{\varnothing,y}]$ and that can be close or not to the tetrahedral Al cation $[(OH)_{\varnothing,Al}$ and $(OH)_{\varnothing,\varnothing}$, respectively] (Fig. 2). In the cases where there are isomorphous cation substitutions in the octahedral sheet, the relative distribution of cations can also alter the equivalence of these OH groups. Besides, the effect of the ^{IV}Al is different if it is in the tetrahedra that are in front of the OH or in the lateral tetrahedra, that is, the ^{IV}Al can be as a first or a third neighbour of the O atom that is in front of the OH group, respectively (Fig. 2e and f).

We can define some geometrical features in order to describe the OH geometry, such as the OH bond length, the orientation angle (ρ) of the OH bond with respect to the (001) plane and the H…O non-bonding distances between the H atoms and the tetrahedral O atoms. Different H…O non-bonding distances can be defined: (1) H_{b1}, that with the O atom that is in front of it and OH…O is contained in a perpendicular plane to the (001) plane; (2) H_{b2} and H_{b3}, that with the basal O atoms that are vicinal to the former one of H_{b1}; (3) H_{a1} and H_{a2}, that with the apical O atoms of the tetrahedra that are approximately in front of it; and (4) H_{a3} and H_{a4}, that with the apical O atoms that are aside to the H atom and belong to the tetrahedra that vicinal to previous ones (Fig. 3).

The main geometrical features of the OH groups for the fully optimized crystal structures are described in Table 3, including the orientation angle (ρ), the OH bond length and the main distances between the hydrogen and the surrounding tetrahedral O atoms. In general, the OH bond length in smectites and illites is higher than in pyrophyllite. The presence of interlayer charge from tetrahedral or octahedral sheet increases the negative charge of the tetrahedral O atoms, increasing the attractive interactions between these oxygens and the hydrogen atoms, and hence it produces an enlargement of the OH bond. Sometimes this effect is quenched by the electrostatic repulsion between the interlayer cation and the hydrogen atom present in the same hexagonal cavity [$d(OH)_{IC,Al} < d(OH)_{\varnothing,Al}$, in $Smec_1$ and $Smec_2$]. In the $(OH)_{x,Al}$ groups, the tetrahedral Al cation can occupy a position that is in front of the H atom and the attractive effect of the tetrahedral oxygens that are in front of the H atom will be higher (H_{b1}, H_{a1} and H_{a2}) in

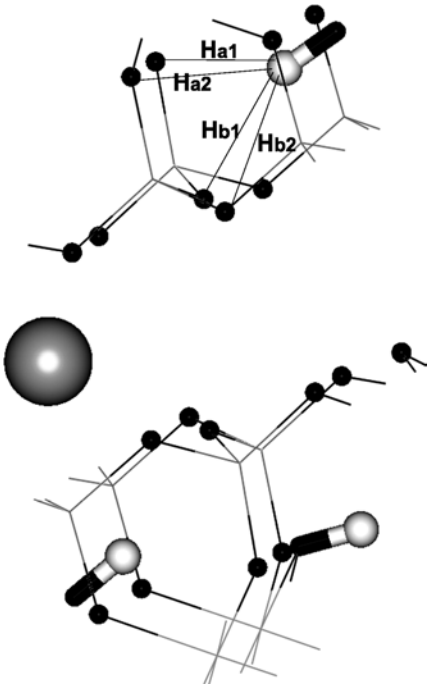

Fig. 3 Non-bonding H…O distances between the H atom and the tetrahedral oxygens. *White* and *black circles* represent H and O atoms, respectively

the O–H bond direction. However, this tetrahedral Al can also occupy a position that is aside of the OH group. In this case, the attractive effect on the H atom does not produce an enlargement of the OH bond, because the non-linear bifurcated hydrogen bonds present a lower strength following the cosine rule (Kerns and Allen 1978) and these interactions are not in the same direction of the O–H bond. However, this $(OH)_{IC,Al}$ bond is also shorter that those OH groups without surrounding Al^{IV} cation, $d(OH)_{IC,Al} < d(OH)_{IC,\varnothing}$. Probably electrostatic interactions of this H atom with the lateral tetrahedral O atoms will be higher (H_{b2}, H_{b3}, H_{a3} and H_{a4}) and hence a slight shortening of the OH bond is observed (Table 3; $d(OH)_{IC,Al} = 0.977$–0.978 Å in $Smec_1$ and $Smec_2$).

The exchange between Na^+ and K^+ as interlayer cations does not produce significant variations in the geometry of the OH groups. The presence of Fe^{3+}-cations in the octahedral sheet produces an enlargement of the OH bond length, following a linear relationship ($R = 0.9998$; Fig. 4). This enlargement could come from the larger electronegativity of Fe^{3+} with respect to Al and Mg, attracting more electrons to it. The higher overlapping between the oxygen orbital and the Fe *d* orbital decreases the electron density in the OH group and the OH bond will be weaker, increasing the OH bond length.

In general, the ρ(OH) angle in pyrophyllite is higher than the average value in the other samples, due to the lack of repulsion with an IC. In the rest of the samples, the OH oriented to the hexagonal tetrahedral cavity with IC adopts a more parallel disposition with a lower ρ(OH) than those that are in the cavity of tetrahedra without interlayer cation [$\rho(OH)_{IC,*} < \rho(OH)_{\varnothing,*}$]. This effect is extremely significant in samples with Fe^{3+} in the octahedral sheet, probably due to the longer *d*(OH) bond length in these samples. When the interlayer charge is high and coming only from the octahedral sheet, the effect of this charge is high and the effect of the

Table 3 Main geometrical features of the OH groups in the crystal structures optimized (distances in Å, and angles in degrees)[a]

Structure	$d(OH)_{x,Al}$	$d(OH)_{x,\varnothing}$	$\rho(OH)_{x,Al}$	$\rho(OH)_{x,\varnothing}$	$(H_{b1})_{x,Al}$	$(H_{b1})_{x,\varnothing}$	$(H_{a1})_{x,Al}$	$(H_{a1})_{x,\varnothing}$	$(H_{a2})_{x,Al}$	$(H_{a2})_{x,\varnothing}$
Pyrophyllite		0.977		33.0		2.10 (166.4)[b]		2.76		2.86
$Smec_1$ $(OH)_{IC,y}$	0.977[c]	0.982	24.8	2.3	2.17 (152.6)[b]	2.66 (123.6)[b]	2.58	2.47	2.65	2.42
$(OH)_{\varnothing,y}$	0.983[d]	0.981	37.9	9.5	2.05 (172.3)[b]	2.46 (135.7)[b]	2.82	2.57	2.83	2.58
$Smec_2$ $(OH)_{IC,y}$	0.978[c]	0.983	24.0	2.3	2.20 (151.6)[b]	2.67 (124.1)[b]	2.57	2.44	2.64	2.47
$(OH)_{\varnothing,y}$	0.983[d]	0.981	38.1	9.9	2.07 (172.5)[b]	2.47 (136.6)[b]	2.82	2.59	2.84	2.59
$Smec_3$ $(OH)_{IC,y}$	0.991[c,e]	0.991[e]	3.2	−5.6	2.66	2.78	2.42	2.37	2.42	2.39
$(OH)_{\varnothing,y}$	0.985[d,f]	0.980[f]	40.8	13.4	2.05	2.40	2.89	2.60	2.90	2.62
$Smec_4$ $(OH)_{IC,y}$	0.993[c,e]	0.992[e]	−2.4	−7.3	2.64	2.78	2.39	2.34	2.39	2.36
$(OH)_{\varnothing,y}$	0.985[d,f]	0.983[f]	40.8	2.0	2.05	2.54	2.85	2.48	2.86	2.49
$Smec_5$ $(OH)_{IC,y}$		0.980[g]		7.5[g]		2.74		2.71		2.74
				−1.3[f]						
$Smec_6$ $(OH)_{IC,y}$		0.979[h]		3.7		2.55		2.38		2.46
$(OH)_{\varnothing,y}$		0.983[f]		2.5		2.58		2.40		2.43
$Smec_7$ $(OH)_{IC,y}$		0.987[i]		−7.7		2.68		2.27		2.41
$(OH)_{\varnothing,y}$		0.982[f]		3.2		2.55		2.41		2.36
$Smec_8$ $(OH)_{IC,y}$	0.984[c,j]	0.986[j]	7.6	−4.6	2.38	2.70	2.47	2.33	2.39	2.46
$(OH)_{\varnothing,y}$	0.983[d,f]	0.981[f]	39.1	7.2	2.07	2.45	2.80	2.52	2.83	2.56

[a] *x* and *y* are variables that have the values, IC or ∅, and Al or ∅, respectively. IC and Al characterize the OH group that is close to the interlayer cation, and to the tetrahedral Al cation, respectively. ∅ represents the lack of the presence of Al or IC close to the OH group

[b] OH. . .O angle

[c] Al^{IV} as a third neighbour of the tetrahedral O atom that is in front of the OH group

[d] Al^{IV} as a first neighbour of the tetrahedral O atom that is in front of the OH group

[e] FeOHFe group

[f] AlOHAl group

[g] MgOHMg group

[h] AlOHMg group

[i] FeOHMg group

[j] FeOHAl group

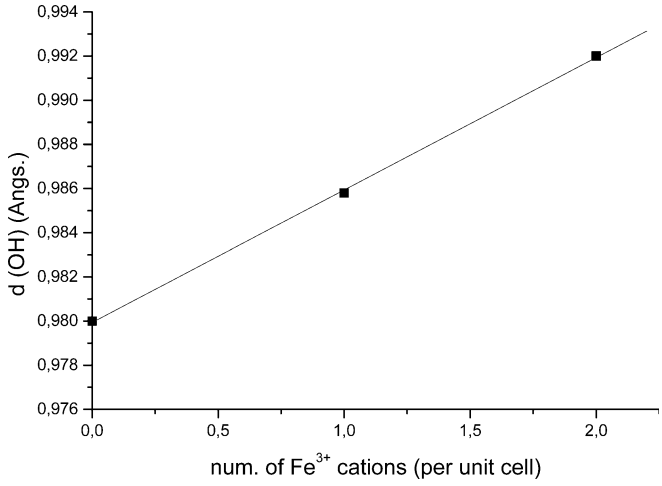

Fig. 4 Effect of the presence of Fe^{3+} cations on the OH bond length

interlayer cation is low and hence the ρ(OH) angle is not so low [$\rho(MgOHMg)_{IC,\varnothing} = 7.5$ ° in $Smec_5$]. In all cases, the presence of tetrahedral aluminium produces a significant increase of ρ(OH) [$\rho(OH)_{*,Al} >> \rho(OH)_{*,\varnothing}$]. The isomorphous substitution of Si^{4+} by Al^{3+} produces an excess of negative charge on the tetrahedral O atoms, increasing the attractive interactions of these O atoms with the hydrogen atoms, and hence increasing ρ(OH). In general, the hydroxyl groups are oriented more parallel to the 001 plane than in trioctahedral clays. These results are consistent with those obtained recently from ab initio molecular dynamics simulations of hydrated montmorillonites (Boek and Sprik 2003).

The presence of the tetrahedral Al increases the strength of the interaction of the H atoms with the tetrahedral O atoms. This distance, H_{b1}, is shorter with no interlayer cation close to the H atom [$(H_{b1})_{\varnothing,Al}$] than with interlayer cation [$(H_{b1})_{IC,Al}$]. The repulsion between the H atom and the interlayer cation slightly decreases the O...H interaction. Besides, in the $(OH)_{\varnothing,Al}$ group, the ^{IV}Al is in the tetrahedra that are in front of this OH group and the effect of this ^{IV}Al will be higher than in the $(OH)_{IC,Al}$ group where the ^{IV}Al is in the lateral tetrahedra, increasing the strength of the H bond and decreasing the value of $(H_{b1})_{\varnothing,Al}$,. However, the differences in H_{b1} do not explain the low value of $d(OH)_{IC,Al}$ bond length, especially if we compare it with the OH groups that have no ^{IV}Al. These OH groups undergo attractive interactions coming from basal and apical O atoms and repulsive interactions with interlayer cations; all these interactions should be taken into account to bring the OH groups to different positions. In $(OH)_{IC,Al}$ the high value of ρ(OH) indicates that the interaction is controlled by the basal tetrahedral O atoms. In this case, these lateral O atoms will have more charge due to the ^{IV}Al presence and the interactions with the OH group will be higher than with the O atoms that are in front of the OH group. In both cases with ^{IV}Al, $(OH)_{x,Al}$, the H_{b1} distance is 0.4–0.5 Å shorter than that in the $(OH)_{x,\varnothing}$ groups The low values of ρ(OH) in $(OH)_{x,\varnothing}$ groups indicates that the interactions are mainly controlled by the H_{ai} distances. Nonetheless, the variation of ρ by rotation of the OH group does not justify the differences in the non-bonding H...O distances. It means that this OH group is not in a fixed position and can be displaced slightly within the flexible MOHM system.

This effect is especially high in samples with octahedral Fe^{3+} ($Smec_3$, $Smec_4$ and $Smec_8$), where the $(H_{b1})_{IC,Al}$ is much higher than $(H_{b1})_{\varnothing,Al}$. A linear relationship is observed between the Fe content per unit cell and the $(H_{b1})_{IC,Al}$ distance ($R = 0.9957$), whereas no effect is observed in the rest of the H_{b1} distances (Fig. 5). In this case, the high length of the OH bond is not due to higher interactions with the tetrahedral O atoms, but due to the electronic structure of the FeOHFe system. This non-bonding distance is directly related with the ρ(OH) angle. The higher ρ(OH) is, the shorter H_{b1}.

A linear relationship is observed between the H_{b1} and the OH...O angle values. However, this relationship is different for long O...H distances than for short O...H distances. In both cases there is a linear correlation, but for short O...H distances the effect of the OH...O angle is higher than for weaker non-bonding O...H interactions, showing two different slopes (Fig. 6). The hydrogen bond strength is inversely proportional to the distance between the two electronegative cations (O...OH), and directly proportional to the cosine of the OHO angle (deviation of the linearity, maximum value at OHO = 180°) (Kerns and Allen 1978). Hence, both geometrical features should give information about the strength of the hydrogen bond involved. Therefore, the two different slopes found in the linear relationships of Fig. 6 indicate two different strength levels of the hydrogen bonds in these clay crystal lattices.

The H_{ai} distances follow the opposite tendency that H_{b1}. The smaller is H_{b1}, the larger is H_{ai}. Analogously, the lower is ρ(OH), the shorter is H_{ai}. The octahedral

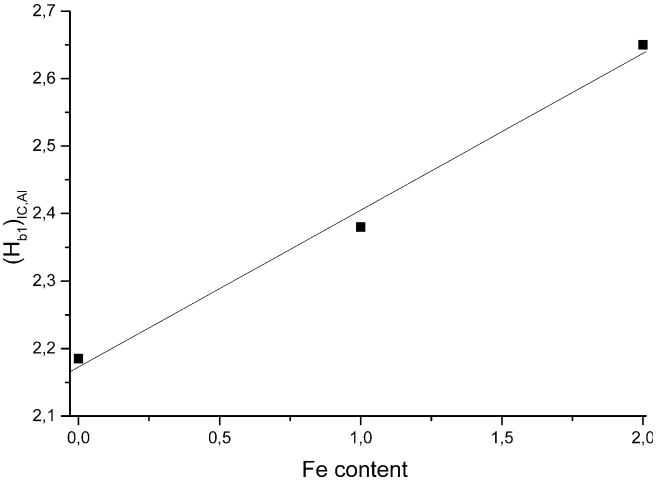

Fig. 5 Relationship between the number of Fe^{3+} cations per unit cell and the $(H_{b1})_{IC,Al}$ non-bonding O...HO distances (in Å)

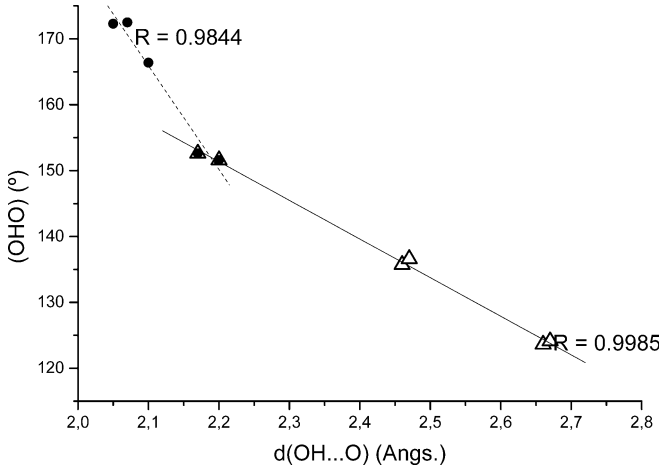

Fig. 6 Correlations between the non-bonding O...HO distances (in Å) and the OHO angle of this interaction (in degrees)

charge produces an increase of the negative charge in the apical O atoms increasing the strength of the interaction of these O atoms with the H atoms, and hence decreasing H_{ai} (Fig. 3). So, in $Smec_5$ H_{b1} and H_{ai} are similar and $H_{ai} < H_{b1}$ in $Smec_6$ and $Smec_7$ samples, due to the low value of ρ(OH). In general, the H_{b2} and H_{b3} distances are larger than former H...O distances and they are in the range 2.8–3.2 Å. In all cases, the OH...O angle is larger in the H_{b1} interactions than in H_{ai} and H_{b2}, H_{b3}.

From this study, we can conclude that the OH groups are not controlled only by the H bond interactions with the H_{b1} distances, but they are inside a cage surrounded by tetrahedral O atoms. Hence, the interactions of all of these O atoms should be taken into account to explore the properties of the OH groups.

Vibrations of OH groups

Although most papers of quantum-mechanical investigations on vibration frequencies applied scaling factors due to the limitations of the Hartree–Fock approach, non-scaled frequencies were used in the most part of the result discussion in this work. The calculated frequencies of the stretching and bending vibration modes of the OH groups are presented along with experimental data in Table 4. Only in this table, the calculated frequencies were scaled for a better understanding in the comparison between calculated and experimental values. Previous authors have found that these corrections are slightly different for high-frequency modes that for low-frequency modes and a dual scaling should be applied to compare with experimental values (Halls et al. 2001). Hence, we use a scaled factor of 1.01 for the stretching frequency ν(OH) (> 1800 cm^{-1}), and a scaled factor of 0.90 for the bending δ(OH) and γ(OH) vibrations (< 1800 cm^{-1}).

Only the atoms of the OH groups participate in the atomic displacements (eigenmodes) of the normal coordinate for ν(OH) vibrations. This means that there is no participation of motions of other atoms in the crystal lattice during this vibration mode. Besides, each type of OH, classified in Table 3, participates independently in a different ν(OH) vibrational normal mode although small contributions of the atomic motions of different OH have been detected in the normal modes of each OH vibration. The analysis of the bending vibration modes of these OH groups presents a main contribution of these OH groups but some small participation of displacements of other atoms was detected, being higher than in the stretching mode.

In pyrophyllite, without octahedral and tetrahedral cation substitutions, the calculated frequency of the stretching vibration, ν(OH), is at 3676 cm^{-1}, matching the experimental values (3675 cm^{-1}, Besson and Drits 1997). The calculated bending-in-plane frequency δ(OH) is at 874, 866 cm^{-1}. Although no experimental data of this vibration were found for pyrophyllite, this calculated value is close to the experimental frequency δ(AlOHAl) reported for smectites (915 cm^{-1}; Cuadros and Altaner 1998). The calculated out-of-plane bending γ(OH) appears at 452 cm^{-1}, close to the frequency

Table 4 Experimental and scaled calculated frequencies (cm^{-1}) of the OH group vibration in smectites and illites

Structure	ν(OH)		δ(OH)		γ(OH) Calc
	Calc	Exp	Calc	Exp	
Pyrophyllite (AlOHAl)	3676	3675[a]	874, 866	915[b]	452
$Smec_1$ (AlOHAl)	3654, 3716	3630, 3680[b], 3675[a]	910, 877	915[c], 914[d]	653
$Smec_2$ (AlOHAl)	3628, 3714	3630, 3680[b]	915	915[c], 914[d]	576, 615
$Smec_3$ ($Fe^{3+}OHFe^{3+}$)	3453, 3465	3505[e]	834, 895	820[f]	663
$Smec_4$ ($Fe^{3+}OHFe^{3+}$)	3427, 3445	3505[e]	833, 894	820[f]	639
$Smec_5$ (MgOHMg)	3693, 3703	3700[d], 3667, 3720[g]	644	669[d]	545
$Smec_6$ (AlOHMg)	3675, 3708	3682[a]	752, 732	820–796[h]	564, 623
$Smec_7$ (FeOHMg)	3548	3543[e]	832	785[f]	574
$Smec_8$ (AlOHFe)	3554, 3545	3573[e]	834	846[f]	600

[a]In montmorillonite (Bishop et al. 1994)
[b]Environment of pyrophyllite in illites (Besson and Drits 1997)
[c]Smectite/illite (Cuadros and Altaner 1998)
[d]Farmer (1974)
[e]Environment of micas in illites (Besson and Drits 1997)
[f]In nontronite (Goodman et al 1976)
[g]In saponites (Pelletier et al 2003)
[h]van der Marel and Beutelspacher (1976)

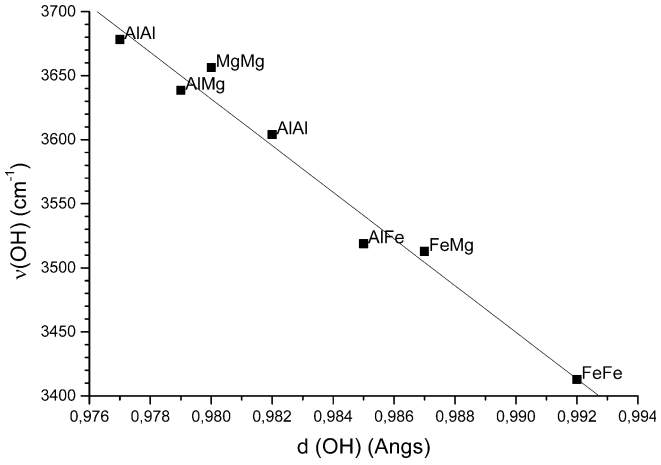

Fig. 7 Relationship between the O–H bond length (in Å) and the non-scaled calculated ν(OH) frequency (in cm^{-1})

obtained from ab initio calculations on clusters related with these minerals (449 cm^{-1}; Sainz-Díaz et al. 2000). These results reinforce the validation of this theoretical approach as a useful tool for experimentalists to predict the assignments of the vibrations of OH groups.

In illite/smectite samples, a good linear correlation ($R = 0.9870$, Fig. 7) between the O–H bond lengths d(OH) and non-scaled theoretical ν(OH) frequencies was found for all samples. The shorter d(OH), the higher is the ν(OH) frequency. This is consistent with previous quantum-mechanical calculations on cluster models representing the octahedral sheet of these minerals (Kubicki and Apitz 1998; Sainz-Díaz et al. 2000).

The effect of the isomorphous substitution of octahedral cations on the calculated ν(OH) frequencies is similar to the experimental behaviour in all cases. A linear relationship ($R = 0.9730$) between the non-scaled calculated values ν(OH) and the experimental data was found in these samples with different cation substitution (Fig. 8). The fitting line intersects in the origin and

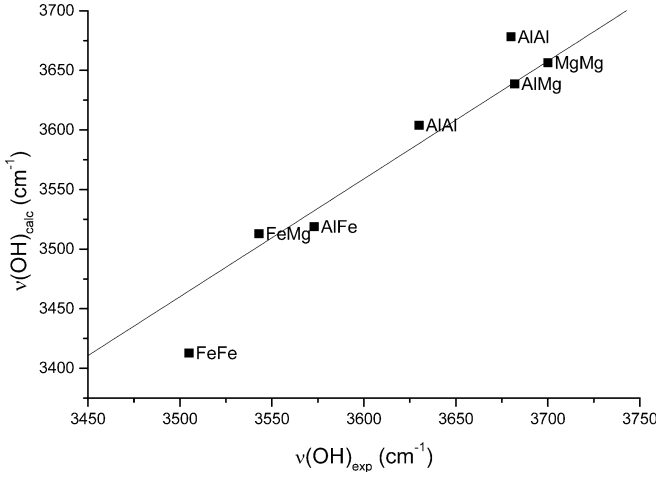

Fig. 8 Effect of the cation substitution on the ν(OH) frequency. Relationship between experimental and non-scaled calculated values (in cm^{-1})

presents a slope close to 1 ($m = 0.99$), indicating a good agreement between the theoretical and experimental values. Previous quantum-mechanical calculations on cluster models yielded a similar conclusion (Timón et al. 2003), where the agreement between theoretical and experimental ν(OH) frequencies was not so good as that in the present work, because the interlayer and tetrahedral cations were not included simultaneously in the cluster models. Therefore, it is necessary to take into account the environment of the whole crystal lattice around these OH groups to investigate properly the vibration properties, including the presence of the interlayer cations and tetrahedral sheet.

The effect of the exchange of interlayer cations Na^+ by K^+ on the frequencies is small (less than 26 cm^{-1}, $smec_1$ versus $smec_2$ and $smec_3$ versus $smec_4$). The samples with K^+ present ν(OH) at slightly lower frequencies than the samples with Na^+. This is consistent with the OH bond length, that is slightly longer in samples with K^+ than in samples with Na^+ (Table 3). This effect is not significant for δ(OH) frequency. However, this effect is important for γ(OH), because the H atom is approaching the interlayer cation during the atomic displacement of this vibration mode. This explanation also justifies the significant difference in the γ(OH) frequency of AlOHAl groups for illites and smectites with respect to that in pyrophyllite, where no interlayer cation is present.

In the samples with only AlOHAl moieties, two groups of frequencies for ν(OH) are detected at 3628–3654 and 3714–3716 cm^{-1}. This is consistent with the two levels of OH bond length detected. The lowest frequency corresponds to the OH groups with the longest OH bond length [$d(OH)_{\varnothing,Al}$, $d(OH)_{\varnothing,\varnothing}$, $d(OH)_{IC,\varnothing} = 0.981$–$0.983$ Å]. The highest frequency corresponds to the $(OH)_{IC,Al}$ group that has the shortest OH bond length [$d(OH)_{IC,Al} = 0.977$ Å] (Table 3). Similar difference in ν(OH) frequency (MgOHMg) was detected experimentally in saponites (trioctahedral 2:1 phyllosilicate with only tetrahedral charge) due to the presence of ^{IV}Al (Pelletier et al. 2003). In this $(OH)_{IC,Al}$ group, the ^{IV}Al is not in the tetrahedra that are in front of the OH group but it is in the tetrahedra that are aside of the OH group, and the H bond interaction H_{b1} will be weaker. Nevertheless, this interaction is still significant observing the low value of $(H_{b1})_{IC,Al} = 2.17$ Å. Therefore, other interactions must be considered to justify this short d(OH) bond length, such as the electrostatic interactions with the aside basal tetrahedral O atoms. However, this $d(OH)_{IC,Al}$ is similar to the d(OH) in pyrophyllite and the ν(OH) frequency is different. The presence of ^{IV}Al increases the electrostatic interactions of the tetrahedral O atoms with the OH group. However, in this $(OH)_{IC,Al}$ group these interactions are not in the same direction of the atomic motions during the normal mode of ν(OH) and hence this vibration will need a higher energy and then a higher frequency. This high ν(OH) frequency for AlOHAl group has not been detected experimentally in smectites and illites due to the

low proportion of ^{IV}Al, and the population of this $(OH)_{IC,Al}$ type for AlOHAl group is very low. The calculated bending-in-plane frequency δ(OH) in $Smec_2$ appears at 915 cm^{-1}, matching the experimental δ(AlOHAl) frequency reported for smectites (915 cm^{-1}; Cuadros and Altaner 1998). In the $Smec_1$ sample this δ(OH) vibration appears at slightly lower frequency with two bands, due to the participation of other atoms of the lattice structure in the atomic motions of the vibration normal mode. The calculated out-of-plane bending γ(OH) appears at higher frequencies than in pyrophyllite due to the presence of the tetrahedral substitution of ^{IV}Al. The atomic motions of the OH atoms during this vibration mode are controlled by the interactions of the hydroxyl group with the tetrahedral O atoms. The presence of ^{IV}Al increases the energy of this vibration mode presenting a higher frequency. The difference in γ(OH) frequency between $Smec_1$ and $Smec_2$ is due to a higher contribution of other atoms of crystal lattice to the atomic motions of this vibration normal mode in $Smec_2$ than in $Smec_1$.

In samples with FeOHFe groups, two ν(OH) frequencies are detected although they are very close each other. They are the lowest values of all samples, independently of the tetrahedral cation substitution. In this case, two OH groups with different environment are detected, although both have similar OH bond lengths. Nevertheless, a slight difference is detected in the non-bonding O…H distances. So, in the $Smec_4$ sample (with K^+ as interlayer cation), the lowest ν(FeOHFe) frequency corresponds to the $(OH)_{IC,Al}$ group [$d(OH)_{IC,Al} = 0.993$ Å, $(H_{b1})_{IC,Al} = 2.64$ Å], and the highest frequency to the $(OH)_{IC,\varnothing}$ group [$d(OH)_{IC,\varnothing} = 0.992$ Å, $(H_{b1})_{IC,\varnothing} = 2.78$ Å]. However, in the $Smec_3$ sample with Na^+ as interlayer cation, both OH groups present identical d(OH) bond length. Analyzing the atomic motions in the vibration mode, a coupling of the vibration of both OH groups to each other is detected and both frequencies are from both FeOHFe groups, corresponding the low and high frequency to the asymmetric and symmetric ν(FeOHFe) vibration modes, respectively. The δ(OH) vibration presents two frequencies for the FeOHFe groups. In this case, the assignment to the OH is the opposite to ν(OH). The lowest δ(FeOHFe) frequency corresponds to the $(OH)_{IC,\varnothing}$ group, and the highest δ(FeOHFe) frequency corresponds to the $(OH)_{IC,Al}$. Both calculated frequencies are higher than those experimentally assigned in nontronites (Goodman et al. 1976). The γ(OH) vibration presents only one band for the FeOHFe groups at higher frequency than pyrophyllite, again due to the presence of ^{IV}Al, as found above in AlOHAl groups.

Two ν(MgOHMg) frequencies are detected from calculations. These frequencies correspond to the coupling of the ν(OH) vibration modes that can be symmetric or asymmetric. Then, the values appeared at 3703 and 3693 cm^{-1} that, taking into account the analysis of atomic motions in the vibration mode, are assigned to the asymmetric and symmetric ν(MgOHMg) vibrations, respectively. This is consistent with the existence of only one environment of these MgOHMg groups in $Smec_5$ (Table 3), because there is no tetrahedral Al and all tetrahedral holes are occupied by interlayer cations. Only one δ(OH) band is detected at a frequency similar to that of the experimental value reported for this MgOHMg group (Farmer 1974). Also only one γ(OH) band was found for this MgOHMg group.

A similar behaviour was found in the ν(AlOHMg) frequencies in $Smec_6$, where two values were detected at 3675 and 3708 cm^{-1}, and only one environment of these AlOHMg groups was found in $Smec_6$ (Table 3). Also two δ(OH) bands were detected in these AlOHMg groups at lower frequencies than those reported experimentally. Similarly, two γ(OH) bands were detected for this AlOHMg group.

Only one ν(FeOHMg) frequency is found in the FeOHMg ($Smec_7$) group calculations reproducing experimental results in mica environments of illites (Besson and Drits 1997). This result is consistent with the only one environment observed in these OH group (Table 3), that is controlled mainly by the H_{a1} and H_{a2} distances. Analogously, only one δ(OH) frequency was found for the FeOHMg system, the calculated one being higher than that assigned experimentally in nontronites (Goodman et al. 1976). In the same way, only one γ(OH) band was detected for these OH groups.

In the group AlOHFe, two ν(OH) frequencies are detected in our calculations. This is consistent with the two environments found for these OH groups in the optimized crystal lattice ($Smec_8$). In both environments, the OH bonds are oriented towards the interlayer cation; however, one has the tetrahedral Al closer than the other (Table 2). Nevertheless, the differences are very small in this case. Again, as in $Smec_1$ and $Smec_2$ samples, the ^{IV}Al cation is not in the tetrahedra that are in front of the OH group, but it is in a lateral tetrahedron. For this reason, the difference in the d(OH) bond length is very small. In both OH groups the H_{b1} non-bonding distances is not the most important and is similar to H_{a1} and H_{a2} distances. Therefore, the ν(OH) vibration mode is controlled by the interactions of several tetrahedral O atoms in the hexagonal cavity. Thus, the high frequency (3554 cm^{-1}) corresponds to the $(OH)_{IC,Al}$ group [$d(OH) = 0.984$ Å] and the low frequency (3545 cm^{-1}) to the $(OH)_{IC,\varnothing}$ group [$d(OH) = 0.986$ Å]. Experimentally, only one ν(OH) band was reported in illites due to the low content in ^{IV}Al and hence a low population of the $(OH)_{IC,Al}$ group. Only one δ(OH) frequency was found for the AlOHFe system, being consistent with the experiment in nontronites (Goodman et al. 1976). Similarly, only one γ(OH) band was found for these OH groups.

Cation substitution effect

Previous experimental studies (Vedder 1964; Robert and Kodama 1988; Besson and Drits 1997, Sainz-Díaz et al.

2000) on the cation substitution effect on the ν(OH) frequency reported that the effect can be related with the change of the mass sum and the valence sum of both cations joined to the bridging OH group. The consideration of the neighbour cation mass effect is merely empiric, because it should assume that there is a certain coupling between the stretching modes of the OH and OM bonds. Calculations of small cluster models by Martínez-Alonso et al. (2002) found that the ν(OH) mode is not strongly coupled to the ν(MO) mode, and they concluded that the mass of the octahedral cations joined to the OH group has no significant effect on the vibration frequencies of this OH group. In our crystal lattice of clay, no significant coupling of the ν(MO) mode with the ν(OH) mode was observed; however, the H atom is not the only one displacing in the stretching vibration mode of the OH group; the oxygen atom is also displacing. Hence a certain contribution of the weight of the cation joined to these oxygen atoms should exist in the reduced mass of the vibration system. Nevertheless, taking into account that this contribution is difficult to quantify, other atomic parameters should be considered in order to justify the experimental behaviour. Martínez-Alonso et al. (2002) justified the variation of the ν(OH) frequency for the cation pairs with the same valence charge sum by the difference in the electronegativity of the cations. However, this parameter presents the opposite effect when pairs of different charges are considered, as in the triad AlAl, AlMg and MgMg. The confusion in the interpretation of these effects comes from the fact that only Al, Mg and Fe are present in our system, and cations with similar atomic properties but higher atomic weight are not present in the octahedral sheet of clays. Nevertheless, in these minerals, the Fe^{3+} has a significantly higher ionic mass than Al and Mg, but at the same time it is a transition metal with a very different valence electronic structure with respect to Al and Mg. Then the apparent consideration of the ionic mass effect can mask other possible effects. Therefore, we conclude that the effect of the Fe^{3+} is due to the presence of *d* orbitals in its valence shell. This fact produces an increase of the electron density along the Fe–O bond, making it more covalent, and less polarized, and hence this oxygen will be less polarized and the OH bond will be longer presenting a lower frequency ν(OH).

Therefore, in order to avoid interference of different atomic parameters, only the triad $Al^{3+}Al^{3+}$, $Al^{3+}Mg^{2+}$ and $Mg^{2+}Mg^{2+}$ should be considered to analyze the effect of the cation valence on the OH vibration frequencies in our samples, without including the Fe^{3+} cation. In Fig. 9 the experimental and non-scaled theoretical ν(OH) frequencies of this triad are plotted with respect to the sum of the valences of the cations joined to these OH groups (cation-pair valence). An increase in the ν(OH) frequency with the decrease in the cation-pair valence is detected for non-scaled theoretical values ($R = 0.9984$), following the same relationship as the experimental frequencies ($R = 0.9872$). This is consistent with the Vedder model (Vedder 1964) and the results reported previously (Martínez-Alonso et al. 2002).

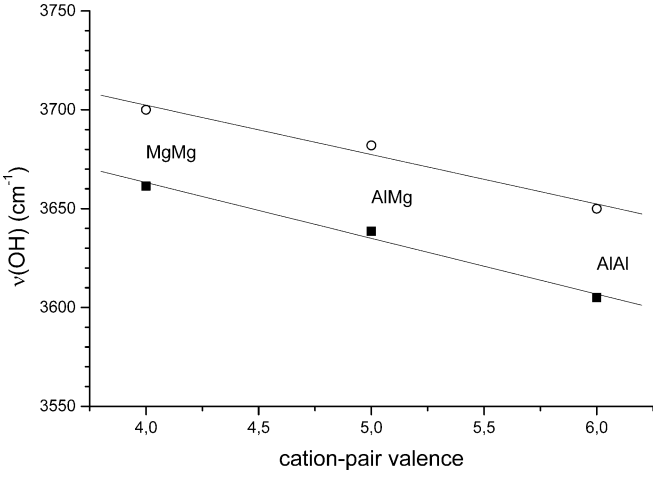

Fig. 9 Effect of the cation-pair valence on the experimental (*hollow symbols*) and non-scaled theoretical (*solid symbols*) ν(OH) frequencies (in cm^{-1})

In Fig. 10, the relationship between the ν(OH) frequencies and the presence of Fe^{3+} cation is represented. A decrease of ν(OH) frequencies with the increase of number of Fe^{3+} cations joined to the OH group is observed for non-scaled theoretical values ($R = 0.9994$), following the same variation as the experimental frequencies ($R = 0.9934$). This relationship is consistent with previous experimental (Besson and Drits 1997) and theoretical (Martínez-Alonso et al. 2002; Sainz-Díaz et al. 2000) works, although the justification is different to that presented in the present work (see above). We consider that this new justification clarifies finally the previous controversy on this point. Further research on similar systems with substitutions of cations with higher atomic weight but without the electronic structure of Fe will be useful to confirm this point.

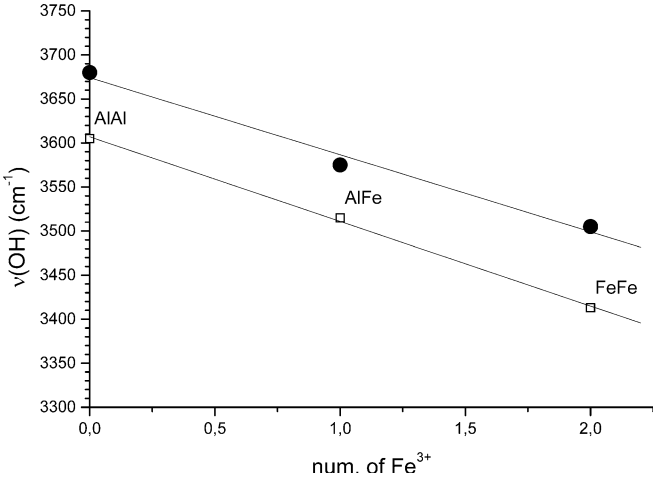

Fig. 10 Relationship between the presence of Fe^{3+} (number of Fe^{3+} cations per unit cell) and the experimental (*solid symbols*) and non-scaled theoretical (*hollow symbols*) ν(OH) frequencies (in cm^{-1})

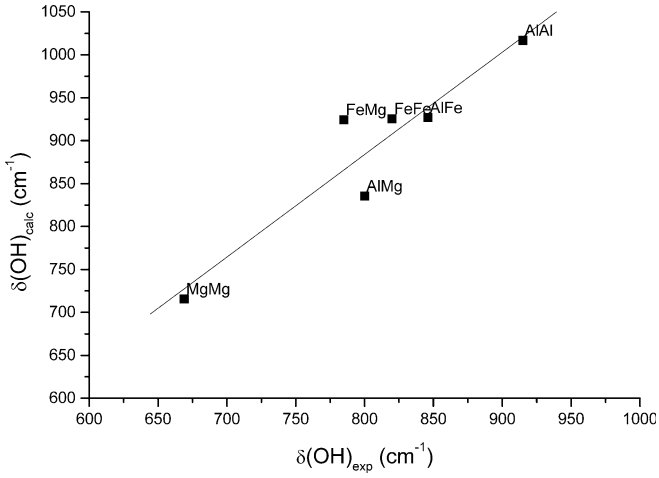

Fig. 11 Relationship between experimental and non-scaled calculated values of δ(OH) frequency (in cm^{-1}) in dioctahedral 2:1 phyllosilicates. Effect of the cation substitution on the δ(OH) frequency

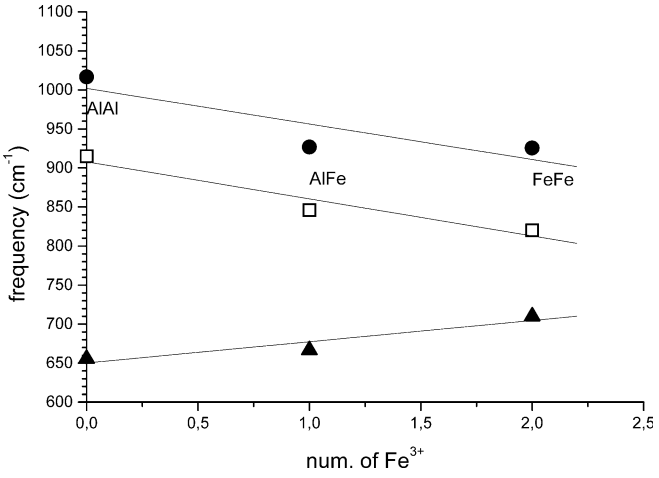

Fig. 13 Experimental (*hollow symbols*) and non-scaled theoretical δ(OH) (*solid circles*) and γ(OH) (*solid triangles*) frequencies (in cm^{-1}) with respect to the presence of Fe^{3+} (number of Fe^{3+} cations per unit cell)

The cation substitution effect on the non-scaled theoretical δ(OH) frequency is similar to that on experimental values, showing a linear relationship (Fig. 11; $R = 0.9382$). The low correlation coefficient of this relationship is due to the dispersion of the experimental values coming from different authors and different natural samples.

The γ(OH) bands (out-of-plane bending vibrations) have not been assigned experimentally in these minerals yet, because they appear in the same region of the M–O–M′ vibrations and structural vibration of the solids and it is difficult to distinguish them. Nevertheless, this vibration mode calculated in this work finds a good agreement with previous calculations on cluster models (Sainz-Díaz et al. 2000).

The non-scaled theoretical δ(OH) frequency increases with the increase of the cation-pair valence in the AlMg triad, following the same relationship that the experimental δ(OH) values (Fig. 12) according to previous work (Sainz-Díaz et al. 2000, Martínez-Alonso et al. 2002). A similar relationship was found in γ(OH), although the slope is lower than in δ(OH) (Fig. 12). This behaviour is the opposite to that for ν(OH). The increase of Fe^{3+} content produces a decrease in the δ(OH) frequency for non-scaled theoretical values, finding a similar relationship in the experimental values (Fig. 13). On the contrary, the opposite effect was observed in γ(OH), the increase of the Fe^{3+} content increases the γ(OH) frequency (Fig. 13).

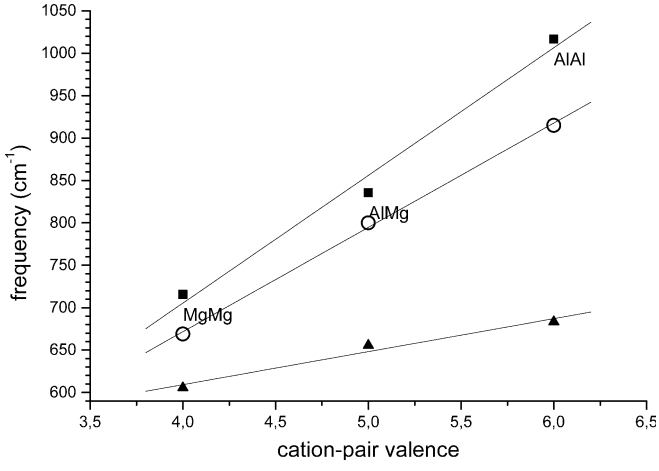

Fig. 12 Effect of the cation-pair valence on the experimental (hollow symbols) and non-scaled theoretical δ(OH) (*solid circles*), and γ(OH) (*solid triangles*) frequencies (in cm^{-1})

Concluding remarks

The vibration of the OH groups depends significantly on the nature of cations which are joined with, and also on the interactions with the tetrahedral O atoms that are surrounding the OH group. These interactions are not only the H bonding with the O atom that is in front of the OH group, but also those with the rest of the tetrahedral O atoms that should be also taken into account within a cage where the OH group is inside. The effect of these interactions has a magnitude similar to the effect of the nature of cation substitution. This means that in many clay structures there is not only one MOHM′ (AlOHAl, FeOHFe, or AlOHMg etc.) frequency, but that different OH frequencies can exist for a certain MOHM′ depending on the environment of each. Many of the differences found by different authors in experimental OH frequencies can come from this phenomenon. Therefore, this conclusion suggests that a wider range of vibrations should be taken into account in the experiment, especially in the assignment of frequencies and determination of relative intensities with the deconvolution analysis method. Recently, Pelletier et al. (2003) have detected different OH environments by using Raman and FT-IR spectroscopy on saponites.

On the other hand, relationships between frequencies and valence state of the cation substitution and the presence of Fe^{3+} found in this work clarify the explanation of the effect of the cation substitution on ν(OH) frequency.

Acknowledgements This work is dedicated in memoriam to Dr. Vicente Botella. The authors are also grateful to E. Artacho for his fruitful discussion, and to the MCYT by the financial support (grants BTE2000-1146-CO2-01 and PPQ2001-2932) and to the Centro Técnico de Informática of CSIC, Centro de Cálculo de la Universidad de Granada, and the computational centre of CIEMAT for allowing the use of their computational facilities. E.E.R. thanks the AECI for her grant for this work.

References

Artacho E, Sánchez-Portal D, Ordejón P, García A, Soler JM (1999) Linear-scaling ab-initio calculations for large and complex systems. Phys Status Solidi 215: 809–817

Bachelet GB, Schlüter M (1982) Relativistic norm-conserving pseudopotentials. Phys Rev (B)25: 2103–2108

Besson G, Drits VA (1997) Refined relationship between chemical composition of dioctahedral fine-grained micaceous minerals and their infrared spectra within the OH-stretching region. Clays Clay Miner 45: 170–183

Bishop JL, Pieters CM, Edwards JO (1994) Infrared spectroscopic analyses on the nature of water in montmorillonite. Clays Clay Miner 42: 702–716

Boek ES, Sprik M (2003) Ab initio molecular dynamics study of the hydration of a sodium smectite clay. J Phys Chem (B)107: 3251–3256

Brindley GW, Brown G. (eds) (1984) Crystal structures of clay minerals and their X-ray identification. Mineralogical Society Monograph no. 5, London

Catti M, Ferraris G, Hull S, Pavese A (1994) Powder neutron diffraction study of 2M1 muscovite at room pressure and at 2 GPa. Eur J Mineral 6: 171–178

Cuadros J, Altaner SP (1998) Compositional and structural features of the octahedral sheet in mixed-layer illite/smectite from bentonites. Eur J Mineral 10: 111–124

Cuadros J, Sainz-Díaz CI, Ramírez R, Hernández-Laguna A. (1999) Analysis of Fe segregation in the octahedral sheet of bentonitic illite-smectite by means of FT-IR, ^{27}Al MAS NMR and reverse Monte Carlo simulations. Am J Sci 299: 289–308

Farmer VC (1974) The layer silicates. In: Farmer VC, (ed) The infrared spectra of minerals. Mineralogical Society, London, pp. 331–363.

Goodman BA, Russell JD, Fraser AR, Woodhams FWDA (1976) A Mössbauer and IR spectroscopic study of the structure of nontronite. Clays Clay Miner 24: 53–59

Guggenheim S, Chang Y-H, Koster van Groos AF (1987) Muscovite dehydroxylation, high-temperature studies. Am Mineral 72: 537–550

Halls MD, Velkovski J, Schlegel HB (2001) Harmonic frequency scaling factors for Hartree–Fock, S-VWN, B-LYP, B3-LYP, B3-PW91 and MP2 with the Sadlej pVTZ electric property basis set. Theo Chem Acc 105: 413–421

Hebenstreit J, Scheffler M (1992) Self-consistent pseudopotential calculations for sodium adsorption on GaAs(110). Phys Rev (B)46: 10134–10145

Hobbs JD, Cygan RT, Nagy KL, Schultz PA, Sears MP (1997) All-atom ab initio energy minimization of the kaolinite crystal structure. Am Mineral 82: 657–662

Kerns RC, Allen LC (1978) Cyclic and bifurcated hydrogen bond. J Am Chem Soc 100: 6587–6595

Kleinman L, Bylander DM (1982) Efficacious form for model pseudopotentials. Phys Rev Lett 48: 1425–1428

Kubicki JD, Apitz SE (1998) Molecular cluster models of aluminum axide and aluminum hydroxide surfaces. Am Mineral 83: 1054–1066

Lee JH, Guggenheim S (1981) Single-crystal X-ray refinement of pyrophyllite-1*Tc*. Am Mineral 66: 350–357

Lee C, Vanderbilt D, Laasonen K, Car R, Parrinello M (1993) Ab initio studies on the structural and dynamical properties of ice. Phys Rev (B)47: 4863–4872

Louie SG, Froyen S, Cohen ML (1982) Nonlinear ionic pseudopotentials in spin-density-functional calculations. Phys Rev (B)26: 1738–1742

Madejová J, Komadel P, Çiçel B (1994) Infrared study of octahedral site populations in smectites. Clay Miner 29: 319–326

Martinez-Alonso S, Rustad JR, Goetz AFH (2002) Ab initio quantum mechanical modelling of infrared vibrational frequencies of the OH groups in dioctahedral phyllosilicates. Part I: Methods, results and comparison to experimental data. Am Mineral 87: 1215–1223

Pelletier M, Michot LJ, Humbert B, Barrés O, D'Espinose de la Caillerie J-B, Robert J-L (2003) Influence of layer charge on the hydroxyl stretching of trioctahedral clay minerals: a vibrational study of synthetic Na- and K-saponites. Am Mineral 88: 1801–1808

Perdew JP, Burke K, Ernzerhof M (1996) Generalized gradient approximation made simple. Phys Rev Lett 77: 3865–3868

Robert JL, Kodama H (1988) Generalization of the correlation between hydroxyl-stretching wavenumbers and composition of micas in the system K_2O–M_2O–Al_2O_3–SiO_2–H_2O: a single model for trioctahedral and dioctahedral micas. Am J Sci 228A: 196–212

Sainz-Díaz CI, Timón V, Botella V, Hernández-Laguna A (2000) Isomorphous substitution effect on the vibration frequencies of hydroxyl groups in molecular cluster models of the clay octahedral sheet. Am Mineral 85: 1038–1045

Sainz-Díaz CI, Timón V, Botella V, Artacho E, Hernández-Laguna A (2002) Quantum-mechanical calculations of dioctahedral 2:1 phyllosilicates: effect of octahedral cation distribution in pyrophyllite, illite, and smectite. Am Mineral 87: 958–865

Sánchez-Portal D, Ordejón P, Artacho E, Soler JM (1997) Density-functional method for very large systems with LCAO basis sets. Int J Quant Chem 65: 453–461

Schindler PW, Stumm W (1987) The surface chemistry of oxides, hydroxides, and oxide minerals. In: Stumm W (ed) Aquatic surface chemistry: chemical processes at the mineral–water interface Wiley Interscience, New York, pp. 83–110

Soler JM, Artacho E, Gale JD, García A, Junquera J, Ordejón P, Sánchez-Portal D (2002) The Siesta method for ab initio order-N materials simulation. J Phys: Condens Matter 14: 2745–58

Stich I, Parrinello M, Holender JM (1996) Dynamics, spin fluctuations, and bonding in liquid silicon. Phys Rev Lett 76: 2077–2080

Timón V, Sainz-Díaz CI, Botella V, Hernández-Laguna A (2003) Isomorphous cation substitution in dioctahedral phyllosilicates by means of ab initio quantum mechanical calculations on clusters. Am Mineral 88: 1788–1795

Tsipursky SI, Drits VA (1984) The distribution of octahedral cations in the 2:1 layers of dioctahedral smectites studied by oblique-texture electron diffraction. Clay Miner 19: 177–193

Troullier N, Martins JL (1991) Efficient pseudopotentials in spin-density-functional calculations. Phys Rev (B)43: 1993–1997

van der Marel HW, Beutelspacher H (1976) Atlas of infrared spectroscopy of clay minerals and their admixtures. Elsevier, Amsterdam

Vedder W (1964) Correlations between infrared spectrum and chemical composition of mica. Am Mineral 49: 736–768